Origin of the Insulating Phase and First-Order Metal-Insulator Transition in 1*T*-TaS_2

Sung-Hoon Lee,[1,*] Jung Suk Goh,[2] and Doohee Cho[2]
[1]*Department of Applied Physics and Institute of Natural Sciences, Kyung Hee University, Yongin 17104, Korea*
[2]*Center for Artificial Low Dimensional Electronic Systems, Institute for Basic Science, Pohang 37673, Korea*

(Received 23 July 2018; revised manuscript received 27 August 2018; published 14 March 2019)

Using density functional theory calculations, we investigate the origin of the insulating phase and metal-insulator transition (MIT) in octahedral tantalum disulfide (1*T*-TaS_2), a layered van der Waals material with a prominent two-dimensional (2D) charge density wave (CDW) order. We show that the MIT is driven not by the 2D order itself, but by the vertical ordering of the 2D CDWs or the 3D CDW order. We identify *two* exceptionally stable 3D CDW configurations; one is insulating and the other is metallic. The competition and mixing of the two CDW configurations account for many mysterious features of the MIT in 1*T*-TaS_2, including the pressure- and doping-induced transitions and the hysteresis behavior. The present results emphasize that interlayer electronic ordering can play an important role in electronic phase transitions in layered materials.

DOI: 10.1103/PhysRevLett.122.106404

Layered materials often show complex electronic phases that depend on temperature, pressure, and doping. They typically show strong 2D charge or spin order owing to the layered atomic structure. Therefore, studies on the physical origin of the complex electronic phases have usually focused on the 2D electronic order. As we will show below, however, the assumption that the interlayer interaction is minor is a preconception that may hinder a correct understanding of the system. For an example of 1*T*-TaS_2, one of the most extensively studied van der Waals layered material, we show that its electronic phase and phase transition are dictated not by the 2D order itself, but by the 3D ordering of the 2D order.

1*T*-TaS_2 is an archetypal 2D charge-density-wave system with a rich electronic phase diagram [1–25]. It shows multiple CDW transitions with decreasing temperature: from a metallic incommensurate phase through a metallic nearly commensurate phase to an insulating commensurate phase with the star-of-David distortion [1,2]. Under doping or pressure, the low-temperature insulating phase undergoes a transition to the metallic phases [3–6]. The metal-insulator transition in 1*T*-TaS_2 is, intriguingly, first order with hysteresis behavior. The zero-temperature electrical resistance depends on cooling rate or external perturbations such as electric currents or laser pulse irradiation [7–11]. The perturbed metallic states persist for a long time at low temperature and were attributed to some "hidden states" [7,8] that are absent in the equilibrium phase diagram [26,27]. The physical mechanisms behind all these phenomena are not well understood.

Theoretically, 1*T*-TaS_2 represents a very interesting model system—a weakly bound solid of 2D triangular lattices of atoms in the d^1 electronic configuration. Each layer of 1*T*-TaS_2 consists of a triangular lattice of Ta atoms of group V, sandwiched between two triangular lattices of S atoms of group VI [Fig. 1(a)]. The resulting triangular lattice of the Ta^{4+} ions in the d^1 configuration is unstable and prone to CDW formation. Experimentally the insulating commensurate CDW phase of 1*T*-TaS_2 exhibits the star-of-David distortion with a $\sqrt{13} \times \sqrt{13}$ periodicity [Fig. 1(b)], where 12 Ta ions among 13 in a unit cell are attracted to each other and produce a CDW band gap. The Ta ion at the star's center has a half-filled nonbonding state with d_{z^2} character at the middle of the band gap. The formation of these localized half-filled states leads to ascribing the insulating phase to a Mott insulator [2].

This conventional description of the insulating phase as a Mott insulator is, however, unsatisfactory for bulk 1*T*-TaS_2, a 3D system of stacked layers. When the star distortion is aligned vertically in the stacked layers, the localized d_{z^2} orbitals of adjacent layers overlap with each other and form an array of vertical 1D chains [Fig. 1(c), *A* stacking]. Although the layers are weakly bound, the overlap is not negligible; the band width of the metallic band along the **c** axis, i.e., perpendicular to the TaS_2 layers, is found to be as large as 0.5 eV [12,13]. This metallic band is robust, regardless of consideration of on-site electronic correlation, leaving the observed insulating phase mysterious [13,14].

Here, we report results of first-principles calculations that uncover the physical origin of the insulating phase and the first-order metal-insulator transition in 1*T*-TaS_2. We carefully examined the vertical stacking order of the 2D CDWs, relaxing the layer spacing for each stacking configuration. We found that the CDW stacking order critically affects the stability and electronic phase of the van der Waals material. Among various possible 3D CDW configurations, two are found to be exceptionally stable.

The ground-state configuration has a double-layer (or paired) stacking configuration. The modulation in vertical CDW alignment for every two layers effectively introduces the Peierls dimerization to the vertical chains of the half-filled localized states, making the system insulating. The second lowest energy configuration is unpaired and metallic, yet very stable owing to a favorable van der Waals interaction and a weak interlayer S—S bonding. We found that the energy difference between the two low-energy CDW configurations is so small that their relative stability can be reversed under moderate pressure or doping, accounting for the pressure- and doping-induced insulator-to-metal transition. We also identified the existence of substantial transition barriers between the two low-energy CDW configurations, which are responsible for the first-order metal-insulator transition and the metastable "hidden states."

Our first-principles calculations were based on the density functional theory (DFT) [29–31] within the generalized gradient approximation (GGA) [32] and included the van der Waals interaction in the Tkatscenko-Scheffler scheme [33]. The electron wave functions were expanded in a plane wave basis set with a cut-off energy of 260 eV. The k-point integration was performed by using a uniform k-point mesh with a mesh density of $4 \times 4 \times 8$ for the Brillouin zone of the $\sqrt{13} \times \sqrt{13} \times 1$ cell. All atoms were relaxed until all the residual forces were less than 0.02 eV/Å. The calculated equilibrium lattice constants for the insulating phase were $a = 3.35$ Å and $c = 5.79$ Å, which are in reasonable agreement with the experimental values of $a = 3.36$ Å and $c = 5.92$ Å [34].

Our study focused on the stacking order of the 2D CDWs, or the 3D CDW configuration. When the center of the star distortion in a reference layer is taken as the A site [Fig. 1(b)], there are 13 center candidates in an adjacent layer, i.e., $A, B, \ldots, M$ sites. Among them, only five are distinct owing to the threefold rotational symmetry: $A \to A$, $A \to B$, $A \to M$, $A \to C$, and $A \to L$. We designate these CDW stacking interfaces simply as A, B, M, C, and L, respectively. The simplest possible 3D configurations are single-layer sliding configurations where a stacking shift occurs for every single layer with the same stacking interface. The five distinct configurations are characterized by stacking vectors of $\mathbf{T}_s = \mathbf{c}$, $\pm\mathbf{a} + \mathbf{c}$, and $\pm 2\mathbf{a} + \mathbf{c}$ (equivalently, $\mp 2\mathbf{a} \mp \mathbf{b} + \mathbf{c}$).

As the origin of the insulating phase, we noted the possibility of the Peierls dimerization [35]: a chain of half-filled atoms is unstable and undergoes atomic dimerization, opening a band gap in the 1D band. For the vertical orbital chains of the present layered system, the dimerization can be achieved effectively by paired stacking, where a stacking shift occurs for every two layers. There are four distinct paired sliding configurations with the unit stacking sequence: AB, AM, AC, and AL.

The calculation results (Table I) show that the CDW stacking order has a dramatic effect on the stability and the

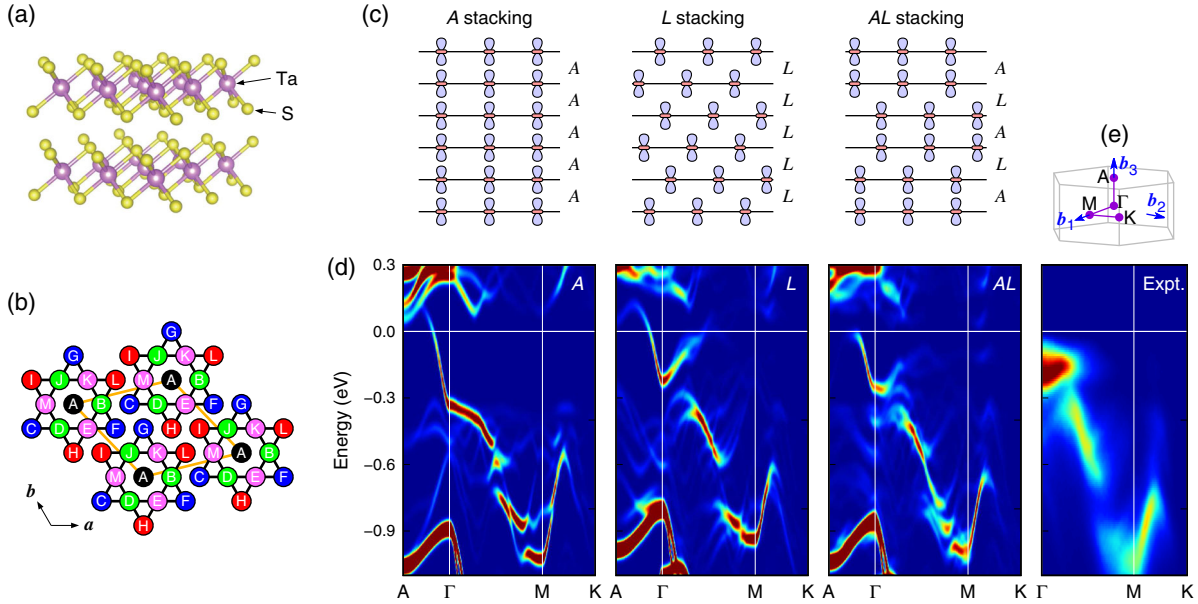

FIG. 1. 3D CDW ordering. (a) Atomic structure of 1T-TaS_2. (b) In-plane star-of-David distortion and labeling convention of the 13 Ta atoms in a star. The Ta atoms at the star center have a half-filled localized state with d_{z^2} character. (c) Arrangement of the localized states of the central Ta atoms for the three representative CDW stacking configurations: A, L, and AL. Side views are shown schematically. (d) Calculated unfolded band structures for the A, L, and AL stacking configurations along the high symmetry line in the Brillouin zone depicted in (e). Experimental ARPES data [17] are shown for comparison. The Fermi level is set to zero. The peak near −1.0 eV around the Γ-A line is from S 3p orbitals, the binding energies of which are underestimated in our GGA calculations and should be located below −1.2 eV [18] (Fig. S1). We used the BANDUP code [28] for band unfolding.

TABLE I. Energy and equilibrium layer spacing as a function of the CDW stacking configuration. The total energy (E_{tot}), equilibrium layer spacing (c), and van der Waals energy (E_{vdW}) are given with respect to the AL stacking configuration.

Unit Sequence	Stacking vector	ΔE_{tot} (meV/star)	Δc (%)	ΔE_{vdW} (meV/star)
A	$\mathbf{T}_s = \mathbf{c}$	53.3	0.54	96.4
B	$\mathbf{T}_s = \mathbf{a} + \mathbf{c}$	46.1	−0.03	−2.6
C	$\mathbf{T}_s = 2\mathbf{a} + \mathbf{c}$	60.7	−0.27	−41.5
M	$\mathbf{T}_s = -\mathbf{a} + \mathbf{c}$	38.5	−0.12	−19.7
L	$\mathbf{T}_s = -2\mathbf{a} + \mathbf{c}$	1.1	−0.43	−74.3
AB	$\mathbf{T}_s = \mathbf{a} + 2\mathbf{c}$	43.3	0.25	43.8
AC	$\mathbf{T}_s = 2\mathbf{a} + 2\mathbf{c}$	34.4	0.21	35.5
AM	$\mathbf{T}_s = -\mathbf{a} + 2\mathbf{c}$	37.4	0.22	39.1
AL	$\mathbf{T}_s = -2\mathbf{a} + 2\mathbf{c}$	0.0	0.00	0.0

equilibrium layer spacing. The total energy of the system varies up to ∼60 meV/star depending on the stacking configuration. The equilibrium layer spacing also changes significantly up to ∼1%, producing large changes in the van der Waals energy of ∼170 meV/star. The calculated total energies show that two configurations are exceptionally stable, the AL and L stacking configurations. They have a small energy difference of 1.1 meV/star but are far more stable than the other configurations (by > 30 meV/star). The ground-state configuration is identified as the AL stacking, a paired configuration with the L stacking interface [36].

The ground-state AL stacking configuration resolves the long-standing puzzle on the origin of the insulating phase of $1T$-TaS_2. The calculated band structure shows the expected band gap [Fig. 1(d)]. The robust metallic band along the Γ-A line with the single-layer stacking configurations shows a gap opening with the double-layer AL stacking. Note that the gap opening of the metallic band occurs along the k_z direction, not in the k_x-k_y plane, as the conventional Mott insulator picture assumes [37]. The band gap of approximately 0.15 eV, obtained using hybrid functional calculations [38] (Fig. S1 in the Supplementary Material [39]), is in good agreement with the optical band gap of 0.1 eV [15]. The unfolded band structure along the Γ-A line with a small band gap matches well with recent k_z-resolved, angle-resolved photoemission spectroscopy (ARPES) data [16], where the occupied metallic band shows no clear band gap for the insulating phase (see Fig. S2). The agreement between the calculation and ARPES experiments is most obvious along the Γ-M-K line, where high-resolution data [17] are available [Fig. 1(d)]. All the key features are well reproduced: a small upward bending of the peak at binding energies around −0.2 eV near Γ, a linear downward band around −0.5 eV in Γ-M, and a check-shape peak around −0.9 eV near M. We note that the good agreement is the characteristic of the L stacking interface, rather than that of the AL configuration. Along Γ-M-K, the band structures of the AL and L configurations are similar to each other, but distinct from that of other A or C configurations (see Fig. S3).

The second lowest energy L stacking configuration is unpaired and metallic. The high stability of the L interface over the other interfaces is surprising. We found that this characteristic is due to two factors: favorable van der Waals interaction and interlayer S—S bonding. By the inward star distortion, S atoms near the star center bulge out by ∼0.2 Å compared to the outer S atoms. The bulging S atoms repel those of adjacent layers. This steric hindrance is largest for the A interface and smallest for the L or C interface ($\mathbf{T}_s = \mp 2\mathbf{a} \mp \mathbf{b} + \mathbf{c}$). This is the major reason why L stacking has a ∼1% smaller layer spacing with a 171 meV/star larger van der Waals energy gain than A stacking. Another important factor is interlayer S—S bonding. In the L interface, two bulging S atoms, each from opposite layers, form a weak π bond with a bond length of 3.2 Å (Fig. S4). This bonding mediates the interlayer coupling between the d_{z^2} orbitals of the adjacent layers. Such interlayer S—S bonding is disallowed at the C interface where the interlayer S—S distance is ∼4.6 Å.

The existence of *two* exceptionally stable stacking configurations, one being an insulator and the other being a metal, suggests that their competition may be responsible for the metal-insulator transition in $1T$-TaS_2. Notable is that the total energy difference between the AL and L stacking configurations is ∼1 meV/star, whereas the van der Waals energy difference between the A and L interfaces is as large as ∼170 meV/star. This indicates that there is a delicate balance between the energy gain by the Peierls-like dimerization and the energy cost in the van der Waals interaction. This implies that the relative stability between the two configurations can be easily changed by doping, which affects the energy gain from the gap opening, or by applying pressure, which affects the layer spacing and thus the van der Waals interaction. We found that this is indeed the case.

We compare the total energies of the AL and L stacking configurations as a function of the layer spacing and electron doping density in Fig. 2. Without pressure or doping, the insulating AL stacking is more stable than the metallic L stacking, with a 0.43% larger equilibrium layer spacing, as already shown in Table I. If pressure is applied to the insulating AL phase at its equilibrium, this layered system would reduce its volume by reducing the layer spacing. As the layer spacing decreases, the AL-stacked phase becomes destabilized and eventually less stable than the L-stacked phase at a 0.35% reduced layer spacing. The critical pressure for this pressure-induced insulator-to-metal transition is estimated to be ∼0.3 GPa [40], which is in reasonable agreement with the experimental value of ∼1 GPa [3,4].

Stability reversal also occurs by carrier doping. As electron doping increases, the minimum total energy of

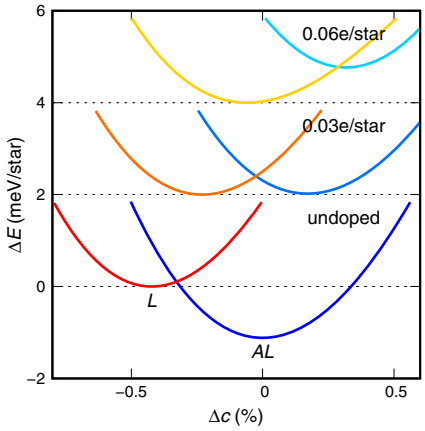

FIG. 2. Dependence on pressure and doping. Total energies of the AL and L stacking configurations are shown as a function of the layer spacing (c) for undoped and electron-doped cases. Relative values are shown with offsets for doped cases.

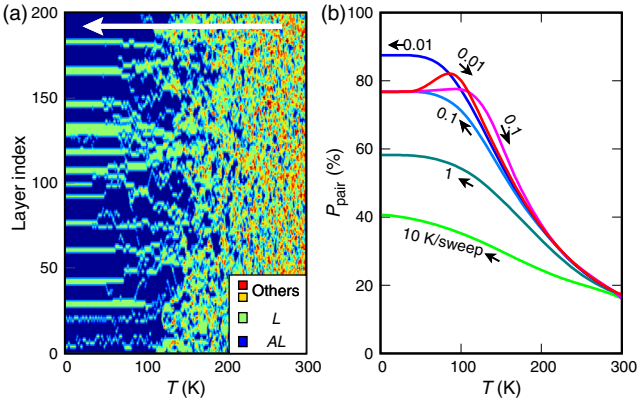

FIG. 3. Hysteresis behavior. (a) Evolution of the CDW stacking configuration under cooling, obtained from the 1D MC simulations. The CDW stacking interfaces for 200 layers are color coded with blue for AL, light green for L, and yellow and red for the other stacking interfaces. The cooling rate was 0.1 K per MC sweep. (b) Population ratio of the AL stacking configuration, P_{pair}, as a function of temperature for various cooling and heating rates. The curves were smoothed to remove fluctuation.

the insulating AL phase becomes higher than that of the metallic L phase (Fig. 2). This occurs because added electrons occupy electronic states that are higher in energy in the former than in the latter by the band gap. The calculated critical doping density of ~0.1 e/star [40] agrees well with the experimental value of 0.1–1 e/star [5,6].

Interestingly, there is a more convincing experimental evidence of this CDW-stacking-driven metal-insulator transition. Two independent measurements of equilibrium lattice constants [34,41] found that, during the transition from the metallic nearly commensurate phase to the insulating commensurate phase at ~180 K, the layer spacing abruptly increases by 0.46–0.49%. This value quantitatively agrees with 0.43%, the difference in equilibrium layer spacing between the metallic L phase and the insulating AL phase. This agreement indicates that the metal-insulator transition in 1T-TaS_2 is indeed due to the competition between CDW stacking configurations.

We now show that there are transition barriers between the two low-energy CDW configurations and these barriers are responsible for the hysteresis behavior of this layered system [7–11]. For this purpose, we performed Monte Carlo (MC) simulations based on an effective 1D model for the interlayer CDW interaction [39]. In this model, each lattice site represents a single TaS_2 layer and is characterized by the position of star centers. The interaction energies between the lattice sites are determined by the stacking interface energies obtained from the DFT calculations (Fig. S5). This model is similar to the Ising model for 1D magnetic transition but has 13 possible states per site instead of two.

Figure 3(a) shows the MC simulation for cooling from 300 K to 0 K with a cooling rate of 0.1 K per MC sweep [42]. Above ~200 K, the CDW stacking configuration is rather random with many unstable stacking interfaces. As temperature decreases below ~120 K, the two low-energy stacking configurations, AL and L, become dominant. Below ~60 K, an interesting feature reveals itself: the stacking configuration is frozen in a mixed configuration of AL and L and fails to arrive at the thermodynamic ground state of the fully paired configuration.

The freezing of the CDW stacking order occurs because of high-energy CDW stacking intermediates on the relaxation path. Consider a stacking segment of -A-L-J-H- in the L stacking configuration, where all the stacking interfaces are the low-energy L interface. A lower-energy AL-stacked segment of -A-A-H-H- can be nucleated by changing the stacking of the middle two layers through an intermediate state of -A-A-J-H- or -A-L-H-H-. Both the intermediate states, however, have a J interface, which is less stable by ~45 meV/star than the initial L interface.

The freezing of the CDW stacking order explains many mysterious observations of 1T-TaS_2. Consider first the cooling-rate dependence of the zero-temperature electrical resistance. Figure 3(b) shows the population ratio of the insulating AL phase, P_{pair}, as a function of temperature for various cooling rates. The zero-temperature P_{pair} is less than 50% when cooled rapidly, and increases as the cooling rate slows down. The simulations indicate that the thermodynamic ground state can be reached only with very slow cooling. Considering that the electrical resistance is roughly exponentially proportional to P_{pair}, the present MC simulations are in good agreement with the experimental observation.

The MC simulations for heating reproduce the hysteresis behavior [Fig. 3(b)]. We started heating at a stacking configuration obtained from a cooling simulation with the cooling rate of 0.1 K per MC sweep. When the heating rate is the same as the cooling rate, the population of the AL domains remains unchanged up to ~120 K, deviating from

the cooling curve at ~50 K. When heated slowly, P_{pair} is further increased at above 50 K, where the system has both thermal energies to overcome low energy barriers and time to find low-barrier paths to thermal equilibrium.

The abnormal response of 1T-TaS_2 to external perturbations can be understood in the same way. For example, when a short laser pulse is irradiated to the insulating phase at low temperature, the electrical resistance drops suddenly and persists for a long time, only rising back to its original values upon heating [7,8]. Our MC simulations of a short heat pulse (Fig. S6) indicate that the metastable "hidden states" are nothing but the frozen mixed phase of the two low-energy 3D CDW configurations.

We thank K. Rossnagel for kindly providing the ARPES data and Ki-Ha Hong, Changwon Park, and Ji Hoon Shim for helpful comments on the manuscript. This work was supported by the National Research Foundation of Korea (Grants No. 2017R1D1A1B03033082 and 2018R1A2B6004044) and by the Institute for Basic Science (Grant No. IBS-R014-D1). Computational resources were supported by the Center for Academic Computing at Kyung Hee University.

*Corresponding author.
lsh@khu.ac.kr

[1] J. Wilson, F. Di Salvo, and S. Mahajan, Adv. Phys. **24**, 117 (1975).
[2] P. Fazekas and E. Tosatti, Philos. Mag. B **39**, 229 (1979); Physica B+C (Amsterdam) **99**, 183 (1980).
[3] B. Sipos, A. F. Kusmartseva, A. Akrap, H. Berger, L. Forró, and E. Tutis, Nat. Mater. **7**, 960 (2008).
[4] T. Ritschel, J. Trinckauf, G. Garbarino, M. Hanfland, M. v. Zimmermann, H. Berger, B. Büchner, and J. Geck, Phys. Rev. B **87**, 125135 (2013).
[5] M. Yoshida, Y. Zhang, J. Ye, R. Suzuki, Y. Imai, S. Kimura, A. Fujiwara, and Y. Iwasa, Sci. Rep. **4**, 7302 (2014).
[6] Y. Yu, F. Yang, X. F. Lu, Y. J. Yan, Y.-H. Cho, L. Ma, X. Niu, S. Kim, Y.-W. Son, D. Feng, S. Li, S.-W. Cheong, X. H. Chen, and Y. Zhang, Nat. Nanotechnol. **10**, 270 (2015).
[7] L. Stojchevska, I. Vaskivskyi, T. Mertelj, P. Kusar, D. Svetin, S. Brazovskii, and D. Mihailovic, Science **344**, 177 (2014).
[8] I. Vaskivskyi, J. Gospodaric, S. Brazovskii, D. Svetin, P. Sutar, E. Goreshnik, I. A. Mihailovic, T. Mertelj, and D. Mihailovic, Sci. Adv. **1**, e1500168 (2015).
[9] A. W. Tsen, R. Hovden, D. Wang, Y. D. Kim, J. Okamoto, K. A. Spoth, Y. Liu, W. Lu, Y. Sun, J. C. Hone, L. F. Kourkoutis, P. Kim, and A. N. Pasupathy, Proc. Natl. Acad. Sci. U.S.A. **112**, 15054 (2015).
[10] M. J. Hollander, Y. Liu, W. J. Lu, L. J. Li, Y. P. Sun, J. A. Robinson, and S. Datta, Nano Lett. **15**, 1861 (2015).
[11] M. Yoshida, R. Suzuki, Y. Zhang, M. Nakano, and Y. Iwasa, Sci. Adv. **1**, e1500606 (2015).
[12] M. Bovet, S. van Smaalen, H. Berger, R. Gaal, L. Forró, L. Schlapbach, and P. Aebi, Phys. Rev. B **67**, 125105 (2003).
[13] P. Darancet, A. J. Millis, and C. A. Marianetti, Phys. Rev. B **90**, 045134 (2014).
[14] T. Ritschel, J. Trinckauf, K. Koepernik, B. Büchner, M. v. Zimmermann, H. Berger, Y. I. Joe, P. Abbamonte, and J. Geck, Nat. Phys. **11**, 328 (2015).
[15] L. V. Gasparov, K. G. Brown, A. C. Wint, D. B. Tanner, H. Berger, G. Margaritondo, R. Gaál, and L. Forró, Phys. Rev. B **66**, 094301 (2002).
[16] A. S. Ngankeu, S. K. Mahatha, K. Guilloy, M. Bianchi, C. E. Sanders, K. Hanff, K. Rossnagel, J. A. Miwa, C. Breth Nielsen, M. Bremholm, and P. Hofmann, Phys. Rev. B **96**, 195147 (2017).
[17] S. Hellmann, T. Rohwer, M. Kalläne, K. Hanff, C. Sohrt, A. Stange, A. Carr, M. M. Murnane, H. C. Kapteyn, L. Kipp, M. Bauer, and K. Rossnagel, Nat. Commun. **3**, 1069 (2012).
[18] E. Lahoud, O. N. Meetei, K. B. Chaska, A. Kanigel, and N. Trivedi, Phys. Rev. Lett. **112**, 206402 (2014).
[19] A. Liu, Phys. Rev. B **79**, 220515 (2009).
[20] X. L. Wu and C. M. Lieber, Phys. Rev. Lett. **64**, 1150 (1990).
[21] K. Rossnagel, J. Phys. Condens. Matter **23**, 213001 (2011).
[22] K. Haupt, M. Eichberger, N. Erasmus, A. Rohwer, J. Demsar, K. Rossnagel, and H. Schwoerer, Phys. Rev. Lett. **116**, 016402 (2016).
[23] C. Laulhé *et al.*, Phys. Rev. Lett. **118**, 247401 (2017).
[24] M. Ligges, I. Avigo, D. Golež, H. U. R. Strand, Y. Beyazit, K. Hanff, F. Diekmann, L. Stojchevska, M. Kalläne, P. Zhou, K. Rossnagel, M. Eckstein, P. Werner, and U. Bovensiepen, Phys. Rev. Lett. **120**, 166401 (2018).
[25] S. Yi, Z. Zhang, and J.-H. Cho, Phys. Rev. B **97**, 041413 (2018).
[26] Y. Tokura, J. Phys. Soc. Jpn. **75**, 011001 (2006).
[27] K. Nasu, *Photoinduced Phase Transitions* (World Scientific, Singapore, 2004).
[28] P. V. C. Medeiros, S. Stafström, and J. Björk, Phys. Rev. B **89**, 041407 (2014).
[29] G. Kresse and J. Furthmüller, Phys. Rev. B **54**, 11169 (1996).
[30] G. Kresse and D. Joubert, Phys. Rev. B **59**, 1758 (1999).
[31] P. E. Blöchl, Phys. Rev. B **50**, 17953 (1994).
[32] J. P. Perdew, K. Burke, and M. Ernzerhof, Phys. Rev. Lett. **77**, 3865 (1996).
[33] A. Tkatchenko and M. Scheffler, Phys. Rev. Lett. **102**, 073005 (2009).
[34] F. Givens and G. Fredericks, J. Phys. Chem. Solids **38**, 1363 (1977).
[35] R. F. Peierls, *Quantum Theory of Solids* (Clarendon Press, Oxford, 1955).
[36] Our calculations showed that a screw variation of the AL stacking configuration with the unit sequence of $ALAIAH$ is more stable by 2.1 meV/star than the sliding configuration. On the other hand, the L stacking configuration prefers sliding to screwing by 12 meV/star.
[37] Earlier ARPES studies [18] claimed that the gap opening occurs on the Γ-M line, i.e., in the k_x-k_y plane (not in the k_z direction), in support of the 2D Mott insulator picture. However, it is ill founded because k_z is not a good quantum number at the crystal surface and thus typical ARPES bands in the k_x-k_y plane are somehow k_z averaged.

[38] J. Heyd, G. E. Scuseria, and M. Ernzerhof, J. Chem. Phys. **118**, 8207 (2003).
[39] See Supplemental Material at http://link.aps.org/supplemental/10.1103/PhysRevLett.122.106404 for figures of detailed band structures, interlayer S—S bonding, and MC simulation methods and results.
[40] For this estimation, we included the stabilizing effect of screwing for the *AL* stacking configuration [36].
[41] O. Sezerman, A. Simpson, and M. Jericho, Solid State Commun. **36**, 737 (1980).
[42] In our MC simulations, the temperature scale is relative because of the 1D approximation [39].